

Experimental evidence for mobile luminescence center mobility on partial dislocations in 4H-SiC using hyperspectral electroluminescence imaging

Joshua D. Caldwell, Alexander Giles, Dominic Lepage, Dominic Carrier, Khalid Moumanis et al.

Citation: *Appl. Phys. Lett.* **102**, 242109 (2013); doi: 10.1063/1.4810909

View online: <http://dx.doi.org/10.1063/1.4810909>

View Table of Contents: <http://apl.aip.org/resource/1/APPLAB/v102/i24>

Published by the AIP Publishing LLC.

Additional information on *Appl. Phys. Lett.*

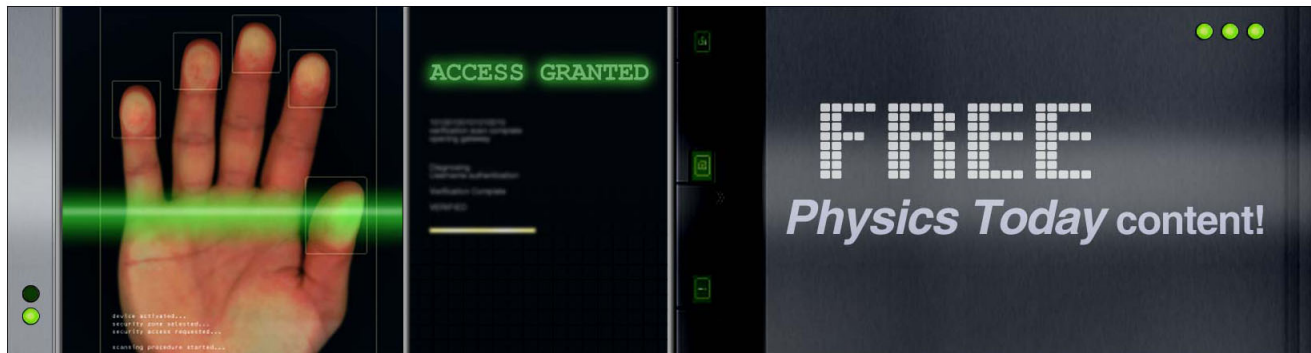
Journal Homepage: <http://apl.aip.org/>

Journal Information: http://apl.aip.org/about/about_the_journal

Top downloads: http://apl.aip.org/features/most_downloaded

Information for Authors: <http://apl.aip.org/authors>

ADVERTISEMENT



Experimental evidence for mobile luminescence center mobility on partial dislocations in 4H-SiC using hyperspectral electroluminescence imaging

Joshua D. Caldwell,^{1,a)} Alexander Giles,² Dominic Lepage,³ Dominic Carrier,³ Khalid Moumanis,³ Brett A. Hull,⁴ Robert E. Stahlbush,¹ Rachael L. Myers-Ward,¹ Jan J. Dubowski,³ and Marc Verhaegen⁵

¹Naval Research Laboratory, 4555 Overlook Ave., S.W. Washington, D.C. 20375, USA

²University of North Carolina at Charlotte, 9201 University City Blvd., Charlotte, North Carolina 28223, USA

³Laboratory for Quantum Semiconductors and Photon-based Bionanotechnology, Department of Electrical and Computer Engineering, Université de Sherbrooke, Sherbrooke, Quebec J1K-2R1, Canada

⁴Cree, Inc., E. Cornwallis Rd., Research Triangle Park, North Carolina 27709, USA

⁵Photon Etc., 5795 Avenue De Gaspe, #222, Montreal, Quebec H2S 2X3, Canada

(Received 17 March 2013; accepted 23 May 2013; published online 19 June 2013)

We report on the formation, motion, and concentration of localized green emission centers along partial dislocations (PDs) bounding recombination-induced stacking faults (RISFs) in 4H-SiC pin diodes. Electroluminescence imaging depicted the motion of these green emitting point defects during forward bias operation along carbon-core PDs that bound the RISFs. Following high temperature annealing, these green emitting point defects did not contract with the PDs, but remained in the final location during the expansion. This implies that the motion of these green emitting point dislocations is enabled through a recombination-enhanced motion, similar to the process for RISF expansion and contraction within SiC. © 2013 AIP Publishing LLC. [<http://dx.doi.org/10.1063/1.4810909>]

Silicon carbide (SiC) based electronic devices have long been desired for high power devices, and high temperature and radiation environments, with the most attention focused on the wide-band gap hexagonal polytypes 4H- and 6H-SiC. More recently, SiC has been demonstrated as a promising material for nanophotonic applications via the optical excitation of surface phonon polariton modes in the mid-infrared (10.3–12.5 μm) as well.^{1–3} Beginning with initial materials science efforts focused on growth and defect characterization beginning in the 1990s, the broad range of extended defects that plagued SiC substrates and epitaxial layers that limited the commercialization of SiC-based electronic devices have been dramatically reduced,⁴ down to levels appropriate for the commercialization of various unipolar devices.⁵ While these efforts have provided significant advancements, extended defects such as threading dislocations,^{6,7} in-grown stacking faults,^{8–11} and recombination-induced stacking faults (RISF),^{2–15} also referred to as Shockley-type stacking faults, which originate from basal plane dislocations (BPDs) persist. In addition, due to the large number of polytypes that have similar formation energies,^{16,17} a wealth of exotic and exciting phenomena can be observed. Perhaps the most interesting phenomenon being the nucleation,¹⁸ expansion,^{19–22} and contraction^{23–27} of RISFs under forward bias, optical injection of free carriers or electron-beam irradiation²⁸ into the low-doped epitaxial drift layers. This process occurs via the recombination-enhanced dislocation glide (REDG) mechanism, whereby the recombination of free carriers near the basal plane dislocations or RISFs provides sufficient energy to originate and propagate kinks along the partial dislocations (PDs) bounding the RISFs.²⁹ This process thus enables these extended defects to not only form but also expand and

contract under various combinations of forward bias and temperature.^{23–27,30} The luminescence response of these defects has been widely reported, resulting in a violet (2.89 eV) and red (1.8 eV) luminescence from the RISF and bounding PDs, respectively,³¹ while another report demonstrated that the PDs also exhibited an additional emission near 1.6 eV.³² Recently, we reported on the observation of green emission from these PDs in several different 4H-SiC devices.³³ Here, we report on the demonstration of the propagation of these green luminescence centers during the forward bias operation of these devices along the C-core PDs, demonstrating the recombination-induced point defect migration (RIPDM) within 4H-SiC pin diodes. Subsequent annealing of the diodes demonstrated that despite the contraction of the RISFs and PDs, these luminescence centers remained, leaving behind a "scarring" of the native lattice, thus demonstrating that this process is indeed due to the motion of these emission centers under forward bias and not due to a structural reconfiguration of the PDs bounding the RISFs. Using electroluminescence (EL) imaging,³⁴ we were able to simultaneously collect the spatial and spectral properties of the extended defects within several diodes, enabling the clear identification of the luminescence band from these defects, something that is not possible with standard measurements. This observation of the RIPDM should enable further insight into the various defect formation and propagation processes within SiC.

The samples used for this work were 4H-SiC pin diodes with a 114 μm thick n^- ($N_D = 2 \times 10^{14} \text{ cm}^{-3}$) drift layer and a 2.5 μm thick p^+ ($N_A = 8 \times 10^{18} \text{ cm}^{-3}$) Al-doped top layer grown epitaxially on an n^+ 4H-SiC 8° offcut substrate. The devices were approximately 1 mm on a side. Full details of the device design can be found in the literature.^{33–35} The top-side electrical contacts were fabricated into a gridded pattern

^{a)}joshua.caldwell@nrl.navy.mil

to provide uniform current spreading while enabling access to the underlying optical emission from the extended defects. It was determined that no observable electrical degradation to the contacts was induced following either the anneal or bias injection. The real-color (RC) EL images were collected via $10\times$ (0.28 NA) or $50\times$ (0.70 NA) Mitutoyo objectives and focused onto an Olympus 750C Ultrazoom camera. RC EL images were collected as a function of time following each successive period of forward bias injection. All images were collected using an injection level of $0.1\text{--}1\text{ A/cm}^2$ for $5\text{--}10\text{ s}$, which was determined not to induce RISF expansion. The current injection to induce RISF expansion was provided via forward bias operation at 12 A/cm^2 for periods ranging from $5\text{--}60\text{ s}$. Following the RISF expansion, the devices were annealed via the method reported by Caldwell *et al.*²⁶ at 700°C for 10 h , which induced a complete contraction of the RISFs and a complete reversal of the forward voltage drift. Following the anneal, the device was subsequently stressed via the same operating conditions.

EL images were collected using a modified version of a commercial system originally designed by Photon Etc.^{34,36} Hyperspectral imaging is achieved by varying the relative position of Volume Bragg Gratings (VBGs) while continuously recording the projected images skewed in the $x\text{-}y\text{-}\lambda$ space.³⁶ Once rectified into orthogonal axes, the stacks of images constitute a hyperspectral cube providing precise information on the spatial and spectral distributions of the EL signal. The images were collected using a $10\times$ Nikon microscope objective, yielding spatial and spectral resolutions down to $1\ \mu\text{m}$ and $4.1\times 10^{-3}\text{ eV}$, respectively. EL was induced through a current injection of 1 A/cm^2 , with an integration time of 20 s for improved signal-to-noise ratio. Consequently, luminescence was spatially monitored over the spectral range of $400\text{ to }780\text{ nm}$.

Presented in Fig. 1 are four RC EL images of one of the 4H-SiC pin diodes used for this study that were collected after (a) 210, (b) 260, (c) 360, and (d) 520 s of current injection at 12 A/cm^2 . These images clearly depict the expansion of the RISFs and the formation and motion of the green luminescence centers along the PDs bounding the faults. A white arrow is provided in each of the images to highlight one such C-core PD. Note that initially, during the RISF expansion, the propagating Si-core PDs give off a bright red luminescence. A similar phenomenon is observed in (a), denoted by the horizontal white arrow, as a dull red luminescence is emitted by the C-core PD created during the RISF expansion. However, under continued injection, the RISF continues to expand and along with it, lengthening that segment of C-core PD until the propagating Si-core PD reaches and intersects with the surface, which occurs following approximately 260 s of current injection [Fig. 1(b)]. Note that as this expansion occurs, the dull red emission of the C-core PD is modified to a bright green color. This green emission was observed to develop along the majority of the C-core PDs within the diode, as well as some unexpanded BPDs and was not attributable to any specific physical interaction of the C-core PD with other defects present. Thus, while in the case of the C-core PD denoted by the arrows in Figs. 1(a)–1(d), the leading Si-core PD (denoted by the yellow vertical arrows), intersected a threading screw dislocation, leading to the splitting of the

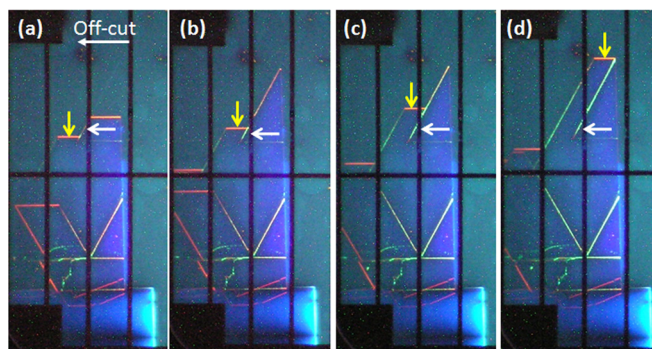


FIG. 1. Real-color electroluminescence images collected after (a) 210, (b) 260, (c) 360, and (d) 520 s of current injection at 12 A/cm^2 . Images were collected under 0.1 A/cm^2 injection for 5 s exposures.

RISF and the formation of a C-core PD³⁷ that eventually developed this green emission, there are several examples within this diode (as well as in other diodes tested) where such interactions were absent. This is clear from the RC EL images presented as well as the time-lapsed video of this RISF expansion that is provided in the supplementary materials online.³⁸ Therefore, this phenomenon cannot be tied directly to such an event, although it is possible that this splitting could assist in the formation of the luminescence centers along the PD. Furthermore, it was observed that the green emission typically developed in such a way that the emission extended along the C-core PD in the same direction as the leading Si-core PD propagation. However, in several examples, the emission develops at the intersection between the Si-core and C-core PDs and develops in a direction anti-parallel to the Si-core propagation. These results seem to imply a gettering of point defects with energy levels deep within the band gap of the SiC rather than the formation of such point defects in the wake of the RISF expansion. In addition, this green EL emission is absent from EL images with injection levels much beyond a few A/cm^2 (not shown). This indicates that the density of states (DOS) for the mid-gap defect (from which this emission originates) is fairly small and thus at higher injection levels becomes saturated. This causes the emission intensity to drop, leaving the EL image and spectra to be dominated by the emission from the defects with a larger DOS and the donor-acceptor band transitions. While broad, diffuse green emission from SiC is common, this bright green EL is only observed along the C-core PDs, further supporting the hypothesis that diffuse point defects within the native lattice coalesce along the PDs during the RISF expansion process. In such a case, it is possible that the kinetic energy from the recombination of electrons with the holes trapped along the PDs would be sufficient to induce such point defect mobility and cause this point defect gettering (coalescence) along the C-core PDs.

Presented in Figs. 2(a)–2(c) are RC EL images of the same diode described above, collected (a) prior to any current injection, (b) following 1980 s of current injection at 12 A/cm^2 , and (c) following a 700°C anneal for 10 h in nitrogen atmosphere to induce the full contraction of the RISFs. By comparing these images, one can observe that following the long current injection experiment, a number of the C-core PDs are induced to emit the aforementioned green

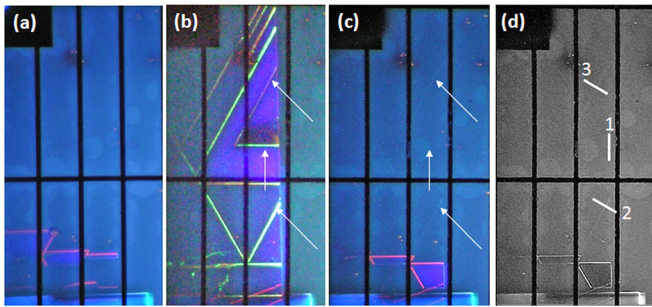


FIG. 2. Real-color electroluminescence images collected (a) prior to, (b) following 1980 s of current injection at 12 A/cm^2 and (c) following 10 h of annealing at 700°C in nitrogen atmosphere. The arrows in (c) denote the locations of the residual "scars" observed following the anneal that coincide with the positions of the green partial dislocations following the current injection. (d) Gray-scale image of the green channel from (c). Inset: gray-scale intensity of the line-scans shown in (d).

EL, as denoted by the arrows in Fig. 2(b). Interestingly enough, following the anneal of this device, while the RISFs and the bounding PDs were contracted back to the initial BPD state, a residual, dull green EL signature remains where the bright green PDs were located just prior to the contraction [arrows presented in Fig. 2(c)]. In order to more clearly observe these residual luminescence lines, a gray-scale image of the green RGB color channel of Fig. 2(c) is provided as Fig. 2(d). By looking back to the initial RC EL image collected from this device prior to any significant current injection [Fig. 2(a)], we can observe that no such emission lines were presented and thus it is clear that these residual sites are directly tied to the green EL centers located along those C-core PDs prior to the anneal. Line-scans of the gray-scale intensity from the three lines presented in Fig. 2(d) across such residual emission "scars" are provided in Fig. 3 and clearly illustrate the residual green emission from these regions. This further supports the idea of a gettering of point defects to the C-core PDs, thereby implying that such point defects have some non-zero mobility under current injection conditions. It is important to note that the green emission was only observed along C-core PDs, which do not propagate and thus do not participate in the REDG mechanism by which the RISFs are known to expand. Therefore, it is possible that a similar RIPDM mechanism exists along C-core PDs, whereby the recombination of carriers instead provides sufficient kinetic energy to induce point defect

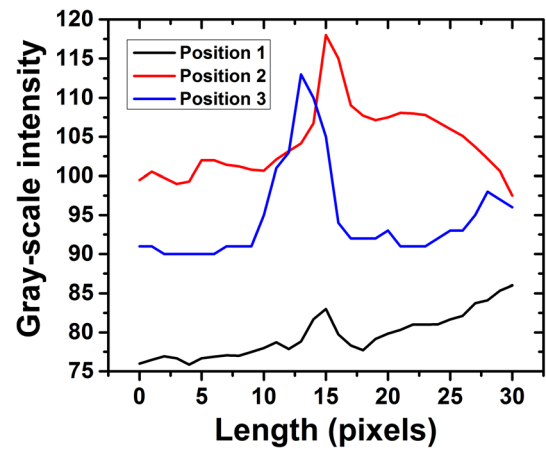


FIG. 3. Gray-scale intensity along lines in Fig. 2(d). Peaks denote the residual green emission from the propagated green emitting point defects following annealing-induced contraction of the RISFs.

motion within the native lattice towards the recombination site. This would explain the coalescence along the C-core PDs that occurs only during forward bias operation.

In an effort to identify a potential point defect that could be providing this green emission, hyperspectral EL imaging was undertaken. Presented in Fig. 4 are selected monochromatic hyperspectral EL images collected at 1 A/cm^2 for 30 s, with the specific center wavelength for each image denoted in the upper right. A RC EL image from this region is provided in the Fig. 4(a) for comparison. As shown in (a) and (b), the RISFs emit at a wavelength roughly centered near 424 nm , which is consistent with the literature.^{4,39,40} The hyperspectral images of the emission from the PDs at (c) 538 nm and (d) 720 nm center pass-bands illustrates that in most cases, these PDs, while appearing predominantly green in color also retain the dull red emission previously correlated with PDs in 4H-SiC.³² This is again supportive of the assertion that the nucleation and coalescence of these green emission centers are due to a RIPDM process, as any physical reconstruction of the PDs would necessarily contract along with the PD during the annealing treatment. Using the hyperspectral technique, one can select a given spatial region and extract the spectrum from the stacked collection of EL images. This was performed on several of the green PDs. Presented in Fig. 4(e) are two spectra derived from the hyperspectral images from the two green emission lines labeled as

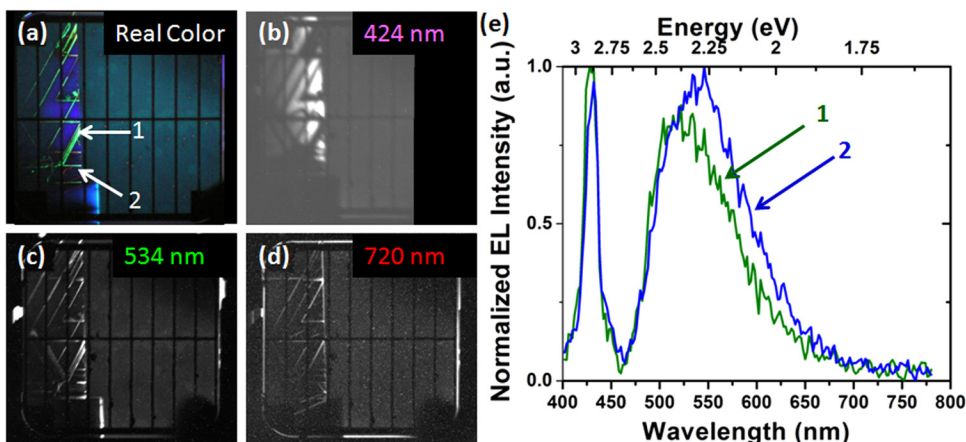


FIG. 4. (a) RC EL and (b)–(d) hyperspectral EL images collected from the same diode following three successive cycles of current injection at 12 A/cm^2 for $\sim 2000 \text{ s}$ and subsequent 700°C , 10 h anneals, followed by a final current injection cycle. The images were collected at 1 A/cm^2 for 5 and 30 s for the real-color and hyperspectral EL images, respectively. The hyperspectral images were collected with the 2 nm pass-band centered at (b) 424 nm , (c) 534 nm , and (d) 720 nm , which correspond to the peak emission of RISFs, the green PDs as observed here and the red PD emission. (e) EL spectra extracted from the series of hyper spectral images of this spatial region.

“1” and “2” in Fig. 4(a). All of the green emitting PDs exhibited a similar spectral response, with a shared EL band near 424 nm associated with the neighboring RISF and a broad EL emission centered near 530–540 nm. Subsequent least squares fitting analysis demonstrate that this broad emission is most likely the emission of two overlapping peaks, which is dominated by one that is centered between 505–515 nm and the another that is broader and located near 540–550 nm. In the case of the former, a similar emission line was reported by Galeckas *et al.*,⁴¹ who observed a spatially diffuse emission around 510 nm that was attributed to boron-related point defects. Previously, based on our coarse determination of the emission wavelength of the emission centers and their coalescence at the C-core PDs, we reported that this was not likely to be the origin of the emission we are reporting on. However, as the hyperspectral imaging enabled the collection of spatially resolved EL spectra, it was determined that the higher energy band of this emission is quite possibly due to boron impurities. It is also possible that this emission is due to an as yet, unidentified point defect that forms under the RIPDM process defined through a coalescence of various point defects currently known. However, efforts at determining the energy associated with these defects through deep-level transient spectroscopy were unsuccessful.

In conclusion, here we report on the observation of mobile green emission centers in 4H-SiC pin diodes. The nucleation and motion of these emission centers was only observed under forward bias operation and only along C-core PDs, implying that the energy provided by carrier recombination at the PDs assisted in the formation and/or mobility of these defect sites. Furthermore, following a subsequent anneal at 700 °C, the RISFs and the bounding PDs were observed to contract back to their original point of nucleation, consistent with the literature.^{23–27,42} However, the green emission centers induced were observed to persist at the point of the green C-core PDs prior to the anneal. This clearly delineated the presence of these green emission sites from any potential reconstruction of the dangling bonds along the C-core PD, instead supporting the hypothesis that this was due to a recombination-induced point defect motion, similar to the recombination-enhanced dislocation glide mechanism by which RISFs are known to expand and contract. Finally, using hyperspectral EL imaging, we were able to identify the spectral response of these spatially localized defects, opening the possibility that this emission is due to mobile boron impurities within the host 4H-SiC lattice.

¹C. F. Bohren and D. R. Huffman, *Absorption and Scattering of Light by Small Particles* (John Wiley & Sons, Inc., Weinheim, Germany, 2004), pp. 331.

²R. Hillenbrand, T. Taubner, and F. Keilmann, *Nature* **418**(6894), 159 (2002).

³J. D. Caldwell, O. J. Glembocki, N. Sharac, J. P. Long, J. O. Owrtsky, I. Vurgaftman, J. G. Tischler, F. J. Bezares, V. Wheeler, N. D. Bassim, L. Shirey, Y. Francescato, V. Giannini, and S. A. Maier, “Low-loss, extreme sub-diffraction photon confinement via silicon carbide surface phonon polariton nanopillar resonators,” *Nano Lett.* (submitted).

⁴M. Skowronski and S. Ha, *J. Appl. Phys.* **99**, 011101 (2006).

⁵J. D. Caldwell, R. E. Stahlbush, and N. A. Mahadik, *J. Electrochem. Soc.* **159**(3), R46 (2012).

⁶R. A. Berehman, M. Skowronski, S. Soloviev, and P. Sandvik, *J. Appl. Phys.* **107**, 114504 (2010).

- ⁷I. Kamata, M. Nagano, H. Tsuchida, Y. Chen, and M. Dudley, *J. Cryst. Growth* **311**, 1416 (2009).
- ⁸J. D. Caldwell, P. B. Klein, M. E. Twigg, R. E. Stahlbush, O. J. Glembocki, K. X. Liu, K. D. Hobart, and F. Kub, *Appl. Phys. Lett.* **89**(10), 103519 (2006).
- ⁹S. Izumi, H. Tsuchida, I. Kamata, and T. Tawara, *Appl. Phys. Lett.* **86**(20), 202108 (2005).
- ¹⁰S. Izumi, H. Tsuchida, T. Tawara, I. S. Kamata, and K. Izumi, *Mater. Sci. Forum* **483–485**, 323 (2005).
- ¹¹S. I. Maximenko, J. A. Freitas, P. B. Klein, A. Shrivastava, and T. S. Sudarshan, *Appl. Phys. Lett.* **94**, 092101 (2009).
- ¹²J. P. Bergman, H. Lendenmann, P. A. Nilsson, U. Lindelfelt, and P. Skyyt, *Mater. Sci. Forum* **353–356**, 299 (2001).
- ¹³R. E. Stahlbush, M. Fatemi, J. B. Fedison, S. D. Arthur, L. B. Rowland, and W. Wang, *J. Electron. Mater.* **31**(5), 370 (2002).
- ¹⁴S. Ha, K. Hu, M. Skowronski, J. J. Sumakeris, M. J. Paisley, and M. Das, *Appl. Phys. Lett.* **84**(25), 5267 (2004).
- ¹⁵A. O. Konstantinov and H. Bleichner, *Appl. Phys. Lett.* **71**(25), 3700 (1997).
- ¹⁶M. H. Hong, A. V. Samant, and P. Pirouz, *Philos. Mag. A* **80**, 919 (2000).
- ¹⁷G. Savini, *Phys. Status Solidi C* **4**(8), 2883 (2007).
- ¹⁸S. Ha, M. Skowronski, and H. Lendenmann, *J. Appl. Phys.* **96**(1), 393 (2004).
- ¹⁹A. T. Blumenau, C. J. Fall, R. Jones, S. Oberg, T. Frauenheim, and P. R. Briddon, *Phys. Rev. B* **68**(17), 174108 (2003).
- ²⁰A. Galeckas, J. Linnros, and P. Pirouz, *Phys. Rev. Lett.* **96**(02), 025502 (2006).
- ²¹S. Ha, M. Skowronski, J. J. Sumakeris, M. J. Paisley, and M. K. Das, *Phys. Rev. Lett.* **92**(17), 175504 (2004).
- ²²N. A. Mahadik, R. E. Stahlbush, J. D. Caldwell, and K. D. Hobart, in *Electronic Materials Conference*, Santa Barbara, CA, 2011.
- ²³J. D. Caldwell, O. J. Glembocki, R. E. Stahlbush, and K. D. Hobart, *Appl. Phys. Lett.* **91**(24), 243509 (2007).
- ²⁴J. D. Caldwell, K. X. Liu, M. J. Tadjer, O. J. Glembocki, R. E. Stahlbush, K. D. Hobart, and F. Kub, *J. Electron. Mater.* **36**(4), 318 (2007).
- ²⁵J. D. Caldwell, R. E. Stahlbush, O. J. Glembocki, M. G. Ancona, and K. D. Hobart, *J. Appl. Phys.* **108**, 044503 (2010).
- ²⁶J. D. Caldwell, R. E. Stahlbush, K. D. Hobart, O. J. Glembocki, and K. X. Liu, *Appl. Phys. Lett.* **90**(14), 143519 (2007).
- ²⁷T. Miyahagi, H. Tsuchida, I. S. Kamata, T. Nakamura, K. Nkayama, R. Ishii, and Y. Sugawara, *Appl. Phys. Lett.* **89**(06), 062104 (2006).
- ²⁸Y. Ohno, I. Yonenaga, K. Miyao, K. Maeda, and H. Tsuchida, *Appl. Phys. Lett.* **101**, 042102 (2012).
- ²⁹K. Maeda and S. Takeuchi, in *Dislocations in Solids*, edited by F. R. N. Nabarro and M. S. Duesbery (North-Holland Publishing Company, Amsterdam, 1996), Vol. 10, pp. 443.
- ³⁰P. Pirouz, *Phys. Status Solidi A* **210**(1), 181 (2013).
- ³¹A. Galeckas, A. Hallen, S. Majidi, J. Linnros, and P. Pirouz, *Phys. Rev. B* **74**(23), 233203 (2006).
- ³²K. X. Liu, R. E. Stahlbush, S. I. Maximenko, and J. D. Caldwell, *Appl. Phys. Lett.* **90**(15), 153503 (2007).
- ³³A. J. Giles, J. D. Caldwell, R. E. Stahlbush, B. A. Hull, N. A. Mahadik, O. Glembocki, K. D. Hobart, and K. X. Liu, *J. Electron. Mater.* **39**(6), 777 (2010).
- ³⁴J. D. Caldwell, L. Lombez, A. Delamarre, G. F. Guillemoles, B. Bourgoin, B. A. Hull, and M. Verhaegan, *Mater. Sci. Forum* **717–720**, 403 (2012).
- ³⁵J. D. Caldwell, A. J. Giles, R. E. Stahlbush, M. G. Ancona, O. J. Glembocki, K. D. Hobart, B. A. Hull, and K. X. Liu, *Mater. Sci. Forum* **645–648**, 277 (2010).
- ³⁶D. Lepage, A. Jimenez, J. Beuvais, and J. J. Dubowski, *Light: Sci. Appl.* **1**, e28 (2012).
- ³⁷Y. Chen, M. Dudley, K. X. Liu, and R. E. Stahlbush, *Appl. Phys. Lett.* **90**(17), 171930 (2007).
- ³⁸See supplementary material at <http://dx.doi.org/10.1063/1.4810909> for time-lapse RC EL video of RISF expansion and corresponding green PD formation.
- ³⁹M. S. Miao, S. Limpijumnong, and W. R. L. Lambrecht, *Appl. Phys. Lett.* **79**(26), 4360 (2001).
- ⁴⁰K.-B. Park, Y. Ding, J. P. Pelz, M. K. Mikhov, Y. Wang, and B. J. Skromme, *Appl. Phys. Lett.* **86**, 222109 (2005).
- ⁴¹A. Galeckas, J. Linnros, and P. Pirouz, *Appl. Phys. Lett.* **81**, 883 (2002).
- ⁴²J. D. Caldwell, O. J. Glembocki, R. E. Stahlbush, and K. D. Hobart, *J. Electron. Mater.* **37**, 699 (2008).